MINING INNOVATION

Open Access

Review Article

A Short Review of Sand Powder 3D Printing in Rock Mechanics

Aoyu Li[1,2], Lishuai Jiang[1,2] ✉, Zhe Zhang[1,2,3], and Hani Mitri[1,2,3,4]

[1] College of Energy and Mining Engineering, Shandong University of Science and Technology, Qingdao 266590, China
[2] State Key Laboratory of Disaster Prevention and Ecology Protection in Open pit Coal Mines, Shandong University of Science and Technology, Qingdao 266590, China
[3] Faculty of Advanced Science and Technology, Kumamoto University, Kumamoto 860 8555, Japan
[4] Department of Mining and Materials Engineering, McGill University, Montreal H3A 0E8, Canada

Cite this article: *Mining Innovation*, **2026**, *1*, 9770002. https://doi.org/10.26599/MI.2026.9770002

ABSTRACT: Sand powder 3D printing has emerged as a promising method for preparing rock-like specimens with controllable geometry and repeatable internal structures. Compared with traditional rock sampling and similar-material casting, this technique can reconstruct fractures, pores, weak planes, and complex discontinuities during digital modeling and printing. It therefore provides a useful experimental approach for studying fracture-controlled deformation and failure in rock mechanics. Building on previous reviews, this short review critically examines the relationship between fracture reconstruction, material-property optimization, and scaled engineering physical modeling. Its contribution lies in distinguishing geometric reproducibility from mechanical similarity, material strengthening from target-specific rock similarity, and laboratory model observations from evidence transferable to engineering prototypes. Particular attention is paid to the effects of matrix materials, printing parameters, particle gradation, and fiber reinforcement on the mechanical behavior of printed rock analogs. The reconstruction of open and infilled fractures, as well as their effects on crack initiation, propagation, and coalescence, is also discussed. Although sand powder 3D printing offers clear advantages in geometric controllability and specimen repeatability, challenges remain in mechanical similarity, natural fracture reconstruction, scale effects, and standardized evaluation. Future studies should combine 3D printing with CT scanning, digital image correlation, acoustic emission monitoring, and numerical simulation to improve its applicability in fractured rock mass research and underground engineering.

KEYWORDS: sand powder 3D printing, rock mechanics, rock analog, fracture reconstruction, mechanical similarity, fractured rock mass

1 Introduction

Natural rock masses contain pores, bedding planes, joints, and fractures at different scales. These discontinuities strongly influence stress redistribution, crack propagation, and macroscopic failure. However, the variability of natural defects makes it difficult to prepare rock specimens with identical internal structures. Conventional methods, including cutting, pre-embedding, and casting, are also limited in their ability to reproduce complex three-dimensional fractures and precisely control their spatial configurations [1, 2]. Therefore, the reproducible fabrication of structurally controlled specimens remains an important challenge in experimental rock mechanics.

Three-dimensional printing provides a digital approach for fabricating rock analogs with prescribed geometries and internal structures. Among the available techniques, sand-based binder jetting, commonly referred to as sand powder 3D printing, is particularly suitable for rock-mechanics research because its granular feedstock and binder-mediated bonding can produce a grain-pore-cementation structure similar to that of some natural rocks [3–5]. The mechanical properties of printed specimens can also be regulated by adjusting the matrix material, particle-size distribution, binder content, printing parameters, and curing conditions.

Sand powder 3D printing also enables direct control of fracture location, size, inclination, number, and spatial arrangement. When combined with computed tomography and three-dimensional reconstruction, it can produce specimens containing complex internal fractures that are difficult to fabricate using conventional methods. This capability provides a reproducible platform for investigating stress concentration, crack interaction, and progressive failure under different loading conditions. Its application has consequently expanded from material-scale testing to physical modeling of layered strata, fractured roadway surrounding rock, and underground support systems [6, 7].

These engineering models also involve openings. Excavation redistributes stress around a roadway or tunnel and creates steep

Received: October 9, 2026; **Revised:** November 9, 2026
Accepted: November 10, 2026

✉Address correspondence to lsjiang@sdust.edu.cn

stress gradients; experimental studies have examined how stress migration and failure mechanisms of rocks with holes depend on multiple stress gradients [8, 9]. A printed model intended to represent roadway stability should therefore reproduce not only the fracture network but also the opening geometry and the stress gradient around it.

Previous reviews have established a substantial foundation for the application of 3D printing in rock mechanics. Gao et al. [10] reviewed different printing materials and their applications, while Yu and Tian [5] specifically examined sand-type materials for artificial rock models and their ability to reproduce selected characteristics of natural rocks. More recently, Jiang et al. [11] reviewed sand-powder-based coal-rock reconstruction and roadway model tests, including material regulation and anchorage applications. Accordingly, the inclusion of sand-based materials, fracture reconstruction, or roadway models alone does not distinguish the present review from previous contributions.

The present review addresses a more focused question: under what conditions does improved fabrication control provide more credible experimental evidence of fracture-controlled rock behavior? To answer this question, it connects three aspects of validation: whether the manufactured fractures reproduce the intended geometry and filling state; whether material optimization improves similarity to a specified rock rather than merely increasing strength; and whether the resulting mechanical behavior can be meaningfully interpreted in scaled models with defined loading and boundary conditions. This critical perspective complements previous application-oriented reviews without assuming that they entirely omitted these issues.

Recent developments provide specific examples for this assessment, including glass-fiber reinforcement [12], particle-gradation optimization [13], internal open-fracture fabrication in a related cement-based binder-jetting system [6], and fractured-roadway physical modeling [7]. By examining these developments together, this review identifies both demonstrated capabilities and unresolved validation requirements. Its intended contribution is a focused synthesis linking fracture reconstruction, material calibration, and engineering interpretation, rather than an exhaustive survey of printing technologies.

2 Sand Powder 3D Printing Technology and Specimen Fabrication

2.1 Applicability of 3D Printing Technologies to Rock Mechanics

Three-dimensional printing enables the direct fabrication of specimens with prescribed geometries and internal defects, providing clear advantages in structural controllability, specimen consistency, and experimental repeatability [10]. The main techniques used in rock-mechanics research include fused deposition modeling (FDM), stereolithography (SLA), selective laser sintering (SLS), and binder jetting (BJT). Their applicability depends not only on geometric accuracy but also on whether the printed specimens can reproduce the deformation and failure characteristics of the target rock.

FDM is inexpensive and convenient, but it generally uses thermoplastic polymers whose ductility and anisotropy differ from those of natural rock. SLA provides high printing accuracy and is suitable for reconstructing complex fractures, although resin-based specimens may exhibit mechanical responses that are not representative of brittle geomaterials. Gypsum- and polymer-based powder printing can reproduce complex structures, but the resulting specimens often have relatively low strength or strong sensitivity to the printing direction.

In comparison, sand-based BJT produces a granular structure in which sand particles are bonded by a selectively deposited binder. The resulting grain-pore-cementation system resembles the internal structure of some porous and weakly cemented rocks. Sand powder 3D-printed specimens can therefore reproduce selected deformation and failure characteristics of coal, mudstone, and sandstone while retaining good geometric controllability and batch consistency [4, 14]. Furthermore, fracture position, inclination, and spatial arrangement can be incorporated directly into the digital model, making the technique particularly suitable for studies of fractured rock masses.

2.2 Printing Principle and Fabrication Process

Sand powder 3D printing is based on binder jetting. During fabrication, a thin layer of sand is first spread across the build platform. A printhead then selectively deposits binder according to the cross-sectional geometry of the digital model. The bonded region forms one layer of the specimen, after which the build platform is lowered and the process is repeated until the complete specimen is produced.

The fabrication process generally includes digital modeling, model slicing, material preparation, layer-by-layer printing, curing, depowdering, and post-treatment [15]. Unlike cutting and casting, this process does not require a physical mold and can incorporate complex internal features into printed specimens. Unbonded powder provides temporary support during printing; however, producing genuinely open internal fractures requires the removal of this powder or other temporary support materials. Internal regions that retain loose powder should therefore be distinguished from open fractures [6].

However, the final mechanical response remains sensitive to particle morphology, particle-size distribution, layer thickness, binder saturation, printing direction, curing conditions, and storage time. Variations in these factors affect particle packing, pore structure, interlayer bonding, and cementation strength. Consequently, accurate geometric reconstruction alone is insufficient. Printing parameters and post-treatment procedures must also be standardized to ensure mechanical consistency between batches and improve the comparability of results from different studies [1, 14, 15].

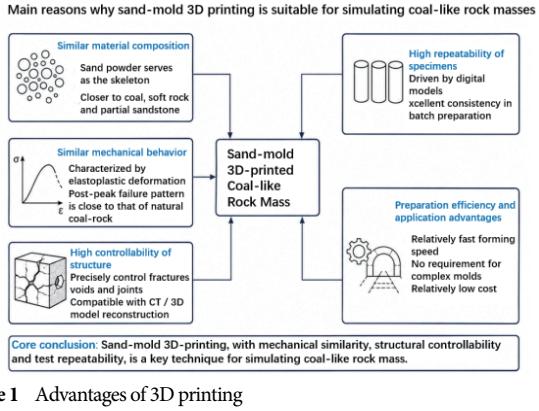


Figure 1 Advantages of 3D printing

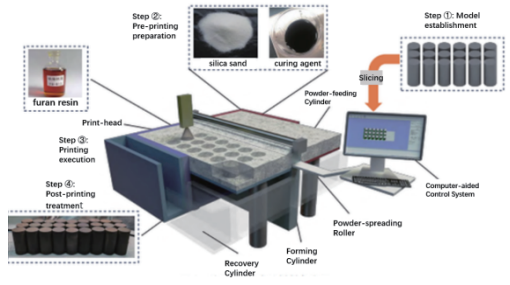


Figure 2 Sand powder 3D printing machine [4]

2.3 Advantages of Sand Powder 3D Printing

The main advantage of sand powder 3D printing is its ability to produce specimens with prescribed and repeatable internal structures. Fracture position, orientation, and arrangement can be defined in a digital model, allowing researchers to vary one geometric feature while keeping the others consistent. This is particularly useful for comparing crack initiation and coalescence in specimens with complex or hidden fractures that are difficult to prepare by cutting or casting [2].

The technique also offers control over material properties. Sand type, particle gradation, binder saturation, and printing parameters can be adjusted to obtain different strength and deformation responses. For example, Jiang et al. [4] demonstrated that sand type and binder saturation substantially affected the mechanical properties and failure behavior of printed weak-rock analogs. At a larger scale, sand printing has been used to prepare roadway models with prescribed fractures and layers of different strengths, enabling repeatable comparisons of surrounding-rock failure [7].

These advantages are most useful when the finished specimen is checked against its intended design. Measured material properties and fracture geometry, including the actual filling state of internal fractures, are needed to establish what the experiment represents. Geometric control and repeatable fabrication thus provide a foundation for rock-mechanics testing; the suitability of each printed model still depends on validation against its target rock and loading conditions.

3 Mechanical Properties and Similarity of Sand Powder 3D-Printed Rock Analogs

3.1 Effects of Matrix Materials and Printing Parameters

The mechanical behavior of sand powder 3D-printed rock analogs is strongly controlled by the matrix material and printing parameters. Particle morphology, surface roughness, binder distribution, layer thickness, and curing conditions jointly determine the bonding quality between sand particles and printed layers. Jiang et al. [4], as summarized by Jiang et al. [16], compared five matrix materials and reported peak compressive strengths of 3.60, 4.45, 6.51, 7.16, and 24.73 MPa for Baozhu sand, quartz sand, GS19 sand, silica sand, and manufactured sand, respectively. Under the reported conditions, the manufactured-sand specimens reached the highest peak strength and displayed a more gradual post-peak decline than the other matrix materials.

Printing parameters also influence specimen quality. A suitable layer thickness improves dimensional accuracy and interlayer bonding, whereas excessive thickness may produce weak interfaces and anisotropic failure. Binder saturation and curing-agent content affect the degree of cementation among particles. Insufficient binder leads to loose structures and low strength, while excessive binder may reduce pore connectivity and alter the deformation mode. Previous studies have shown that proper optimization of these parameters can significantly improve the strength, stiffness, and failure characteristics of printed specimens, making them closer to weak rocks such as coal, mudstone, and soft sandstone [1, 14, 15].

3.2 Particle Gradation and Fiber Reinforcement

Although sand powder printing has good geometric controllability, the high initial porosity of printed specimens often limits their strength and elastic modulus. Particle gradation is an effective method for improving packing density. By combining coarse particles as the load-bearing skeleton and fine particles as pore fillers, the internal structure becomes denser and the contact area between particles increases. For example, gradation optimization based on the Andreasen model has been reported to increase the uniaxial compressive strength from 24.73 MPa to 34.31 MPa and the elastic modulus to about 4.05 GPa [13]. This indicates that particle packing is a key factor in regulating the mechanical similarity of printed rock analogs.

Fiber reinforcement provides another route for enhancing mechanical performance. Short glass fibers can bridge microcracks, transfer stress, and delay crack coalescence during loading. An appropriate fiber content improves both strength and stiffness; for instance, a fiber content of about 10% has been reported to increase

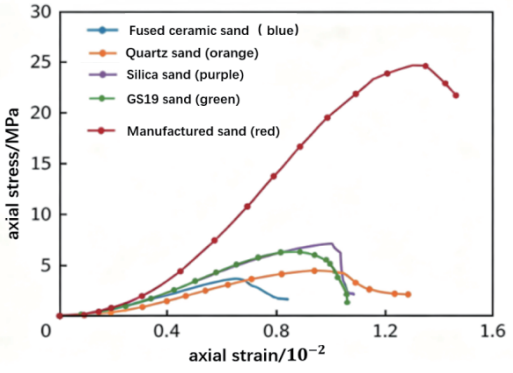


Figure 3 Stress–strain curves for five matrix materials (data from Jiang et al. [4], adapted from Fig. 2 of Jiang et al. [16]). The purple, blue, and red curves represent silica sand, fused ceramic (Baozhu) sand, and manufactured sand, respectively.

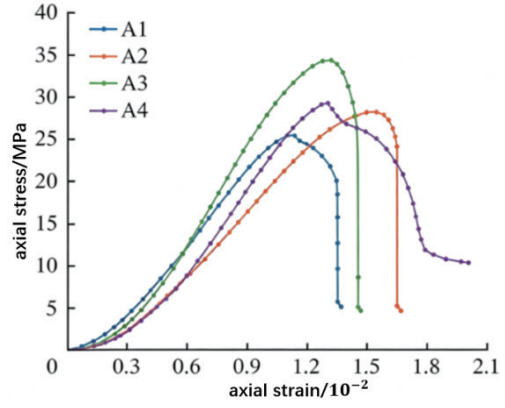


Figure 4 Stress-strain curves for different particle-size groups [13]

the uniaxial compressive strength to 35.18 MPa and the elastic modulus to 4.15 GPa [12]. However, excessive fiber addition may cause fiber agglomeration, weak fiber-matrix interfaces, and nonuniform stress distribution. Therefore, fiber reinforcement should be optimized rather than simply increased.

3.3 Mechanical Similarity and Rock-Type Applicability

Mechanical similarity between sand powder 3D-printed specimens and natural rocks should be evaluated using a combination of compressive strength, tensile strength, elastic stiffness, brittleness, and post-peak response. These indicators describe different aspects of mechanical behavior and should not be treated as interchangeable. Matching uniaxial compressive strength alone does not establish similarity in tensile cracking, deformation, or failure evolution. Accordingly, this review recommends evaluating both individual properties and their relationships, particularly the compressive-to-tensile strength ratio (σ_c/σ_t) and the stiffness-to-strength ratio (E/σ_c), with consistent units and testing procedures. Agreement in these ratios is useful but remains insufficient without comparison of stress–strain curves and failure mechanisms.

Comparisons of printed specimens with natural sandstones show that mechanical similarity depends on the material system and on the properties being evaluated [17, 18]. Perras and Vogler [17] compared printed specimens with three natural sandstones and found that quartz sand specimens bonded with furan resin most closely resembled the weak sandstone. Their results also showed similarities in strength–stiffness and compressive–tensile strength relationships. However, some other printed material combinations exhibited fracture patterns uncommon in natural specimens. Thus, similarity depends on the material system and target rock rather than on compressive strength alone. When optimizing binder content, particle gradation, or reinforcement, tensile strength should therefore be measured alongside compressive strength to determine whether the desired strength ratio is preserved. Direct and indirect tensile results should also be distinguished when comparing studies.

Brittleness and post-peak behavior require separate evaluation because neither is fully represented by peak strength or a strength ratio. Xu et al. [15] reported that specimens printed with a layer thickness of 0.2 mm exhibited a peak compressive strength of 4.45 MPa and a residual strength of 2.20 MPa, whereas those printed with a layer thickness of 0.3 mm exhibited corresponding values of 1.83 and 1.49 MPa. These values imply residual-to-peak strength ratios of approximately 0.49 and 0.81, respectively. The thinner-layer specimens therefore displayed a substantially greater relative post-peak strength loss within that experimental system. This example shows that printing parameters can alter both load-bearing capacity and failure characteristics; strength improvement should consequently be assessed together with changes in post-peak response.

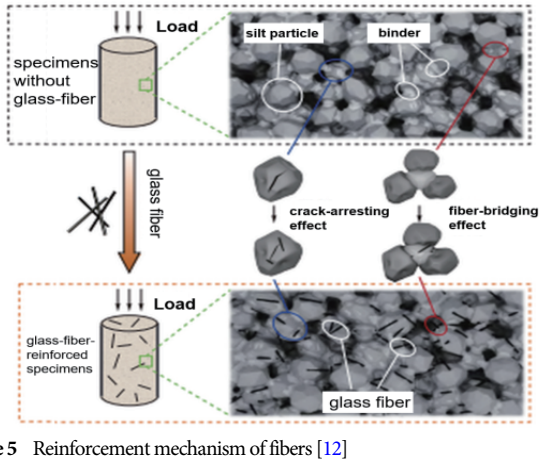


Figure 5 Reinforcement mechanism of fibers [12]

For systematic comparison, this review proposes reporting the definition of each brittleness index, peak strain, post-peak softening, residual-to-peak strength ratio, and observed fracture pattern. Residual strength should be evaluated at a specified deformation level, and comparisons should account for specimen geometry, loading direction, confinement, loading rate, and testing control. A material that matches peak strength but retains excessive post-peak load-bearing capacity may be unsuitable for reproducing abrupt brittle failure. Conversely, reproducing a sudden stress drop does not establish similarity in tensile strength or elastic stiffness. Material optimization should therefore seek a compatible set of properties for the intended failure process rather than maximize any single indicator. Applicability should consequently be defined by the target behavior as well as the rock type. The direct comparison by Perras and Vogler [17] supports the use of sand–furan specimens as analogues of weak sandstone under the investigated conditions; it does not establish equivalence across all sandstones. For coal or other bedded rocks, strength matching should be supplemented by verification of directional properties and bedding-controlled failure. Likewise, low compressive strength alone cannot establish suitability for mudstone applications involving water sensitivity or time-dependent deformation. For strong, dense rocks such as granite and basalt, full mechanical equivalence should remain unclaimed unless stiffness, tensile resistance, brittleness, and post-peak behavior are jointly validated. In scaled engineering models, lower absolute specimen strength may nevertheless be acceptable when the required similarity relationships are satisfied [19]. The intended use should therefore be stated explicitly as reproduction of intact-rock behavior, investigation of selected fracture mechanisms, or scaled physical modeling. Table 1 summarizes these indicators for the printed material systems reviewed in this section and relates them to the natural rocks used as targets.

Tensile strength is the missing indicator in this dataset: σc/σt cannot yet be evaluated across the reviewed material systems, and direct tensile or Brazilian tests are needed to establish whether the optimized materials preserve the compressive-to-tensile balance.

3.4 Quantitative Comparison and Applicable Conditions

Table 2 compares selected printing materials, processing parameters, and mechanical properties of sand-based 3D-printed rock analogs. The comparison distinguishes material selection, binder regulation, layer thickness, particle gradation, and fiber reinforcement. Fabrication and testing conditions are included because differences between studies prevent the reported strengths and elastic moduli from being interpreted as a direct ranking of material performance.

The comparison shows that strength and stiffness do not necessarily respond proportionally to processing changes. In Jiang et al. [4], increasing binder saturation from 25% to 100% increased UCS by approximately 406%, whereas elastic modulus increased by approximately 132%, calculated from the reported means. Binder adjustment therefore cannot be assumed to achieve simultaneous

Table 1 Compressive strength, elastic modulus, stiffness-to-strength ratio, post-peak response, and natural-rock comparison of sand powder 3D-printed coal-like materials

Material system	UCS/E (MPa/GPa)	E/σ_c ($\times 10^{-3}$)	Post-peak response and natural-rock comparison
Baozhu sand [4]	3.60 / 0.50	0.139	Sharp drop after peak; not compared
Quartz sand [4]	4.45 / 0.45	0.101	Sharp drop after peak; not compared
GS19 sand [4]	6.51 / 0.81	0.124	Sharp drop after peak; not compared
Silica sand [4]	7.16 / 0.79	0.110	Sharp drop after peak; not compared
Manufactured sand [4]	24.73 / n.r.	n.r.	Gradual decline after peak; not compared
Gradation-optimized A3 [13]	34.31 / 4.05	0.118	Brittle, sharp post-peak; slightly below red sandstone and shale, above fine sandstone and coal
Fiber-reinforced 10% [12]	35.18 / 4.15	0.118	Brittle, sharp post-peak; above the compared natural rocks

E/σc = elastic modulus/UCS; n.r. = not reported. "Not compared" indicates that the material was not included in the natural-rock stress–strain comparison. Post-peak descriptions follow the reported stress–strain curves. Tensile strength was not reported in these compression tests.

Table 2 Comparison of printing materials, processing parameters, and mechanical properties of sand-based 3D-printed rock analogs

Reference and investigated factor	Printing materials and key parameters	Compressive strength (MPa)	Elastic modulus (GPa)	Applicable conditions and limitations
Jiang et al. [4]: matrix material	Baozhu sand; quartz sand; GS19 sand; silica sand; manufactured sand. Furan resin; binder saturation 55%	3.60; 4.45; 6.51; 7.16; 24.73, respectively	0.50; 0.45; 0.81; 0.79; n.r., respectively	Representative responses from 50 × 50 × 100 mm prisms tested at 0.3 mm/min. Manufactured sand produced the highest strength; its elastic modulus was not reported.
Jiang et al. [4]: binder saturation	Silica sand–furan resin; binder saturation 25%, 50%, 75%, and 100%	Mean values: 3.06; 5.23; 9.16; 15.49	Mean values: 0.38; 0.42; 0.84; 0.88	Four specimens per condition; same prism geometry. Saturation settings are specific to the reported printing system.
Jiang et al. [16]: curing-agent content	Manufactured sand; layer thickness 0.2 mm; binder saturation 100%; curing-agent mass fractions of 0.3%, 0.6%, and 0.9%	27.39 at 0.6%	6.25 at 0.6%	0.6% gave the highest strength and stiffness in the tested range.
Xu et al. [15]: layer thickness	Quartz sand, 0.075–0.120 mm; furan resin; layer thicknesses of 0.2, 0.3, and 0.4 mm	Reported peak values: 4.45; 1.83; 0.78	n.r.	50 × 50 × 100 mm prisms; natural solidification for 3–4 days; loading at 0.3 mm/min. Layer thickness also affected the binder-to-sand ratio.
Wang et al. [14]: grain mixture	Silica sand–furan resin; coarse-to-fine sand mass ratios of 100:0, 70:30, 50:50, 30:70, and 0:100; layer thickness 0.2 mm; reported default binder-saturation setting of 10%	Mean values: 8.53; 8.22; 7.92; 7.45; 6.52	n.r.	Median coarse- and fine-sand grain sizes of 190 and 120 μm, respectively; Ø50 × 100 mm cylinders; drying at 80°C; loading at 0.05 kN/s. The reported 10% binder-saturation setting should not be directly compared with settings used in other studies.
Wang et al. [14]: layer thickness	Coarse silica sand–furan resin; layer thicknesses of 0.2, 0.3, and 0.4 mm	Mean values: 8.49; 6.12; 2.82	n.r.	Other conditions as above. This is a separate experimental series from the grain-mixture comparison.
Particle gradation: Zhang et al. [13], as summarized by Jiang et al. [16]	Manufactured sand; layer thickness 0.2 mm; binder saturation 100%; curing-agent mass fraction 0.6%; optimized Andreasen exponent α = 0.5, group A3	24.73 for single-size-range group G2; 34.31 for optimized group A3	4.05 for A3; n.r. for G2	Text-reported uniaxial compression results. The optimum applies to the investigated grading and processing conditions.
Glass-fiber reinforcement: Jiang et al. [12], as summarized by Jiang et al. [16]	Silica sand, 0.075–0.150 mm; layer thickness 0.20 mm; binder saturation 100%; curing-agent mass fraction 0.6%; fiber contents of 0–12%	13.93 without fibers; 35.18 at 10% fiber content	1.98 without fibers; 4.15 at 10% fiber content	Maximum reported performance at 10%; deterioration above this content. The mass/volume basis of fiber content is not explicitly defined in the cited section.

Notes: n.r. = not reported in the source used for this table. Values separated by semicolons follow the material order in the same row. Reported peaks, representative responses, and group means carry different statistical meanings and are not ranked directly across studies.

strength and stiffness matching.

The two layer-thickness studies show a consistent direction of change but different magnitudes. Increasing thickness from 0.2 to 0.4 mm reduced strength by approximately 82.5% in Xu et al. [15] and 66.8% in Wang et al. [14]. These findings support thinner layers within the tested ranges, rather than a universal optimum. Differences in feedstock, binder dosage, curing, specimen geometry, and loading protocol prevent the between-study strength differences from being attributed to layer thickness alone. Furthermore, Wang et al. [14] found that increasing the fine-sand fraction reduced strength within their selected blends, indicating that adding finer particles does not necessarily improve mechanical performance.

The particle-gradation results of Zhang et al. [13] and the glass-

fiber results of Jiang et al. [12], as summarized by Jiang et al. [16], extend the comparison to optimized material formulations. The text-reported strength increased from 24.73 MPa for group G2 to 34.31 MPa for the optimized gradation group A3, corresponding to an increase of approximately 38.7%. In the fiber series, strength increased from 13.93 MPa without fibers to 35.18 MPa at 10% fiber content, corresponding to an increase of approximately 152.5%, while elastic modulus increased from 1.98 to 4.15 GPa. However, the different reference specimens prevent these percentages from establishing the superiority of one enhancement method over the other.

For practical application, Table 2 should be used to identify candidate formulations and processing ranges for further calibration. Parameter selection should consider the target rock's stiffness, tensile behavior, failure pattern, and post-peak response alongside compressive strength. Comparisons should also account for specimen geometry, loading orientation and rate, curing history, and the definition used to calculate elastic modulus. Where these conditions differ or remain incompletely documented, the reported optimum should be treated as study-specific rather than directly transferable to another printing system or engineering model.

4 Reconstruction of Fractured Rock Masses and Fracture-Controlled Failure

4.1 Reconstruction of Open Fractures

Fractures are among the most important defects controlling the mechanical behavior of rock masses. In conventional laboratory tests, it is difficult to prepare specimens with identical fracture geometry, especially when the fractures are curved, branched, rough, intersected, or distributed in three dimensions. Sand powder 3D printing provides a practical solution to this problem because fractures with different shapes and spatial arrangements can be introduced during model design and printed with high geometric repeatability [1, 6, 20].

Existing studies have used sand powder 3D printing to prepare specimens containing single fractures, multiple parallel fractures, cross fractures, and complex fracture networks. The fracture angle, length, spacing, number, and spatial position can be independently controlled. This makes it possible to clarify how fracture geometry affects crack initiation, propagation, coalescence, and final failure. Under compressive loading, tensile wing cracks may initiate from fracture tips, while secondary shear cracks and splitting cracks can develop as loading continues. The crack evolution and final failure mode depend on fracture geometry, spatial distribution, and loading conditions. Under dynamic loading, fracture dip angle, number, and distribution also influence dynamic peak stress and dynamic elastic modulus [20–22].

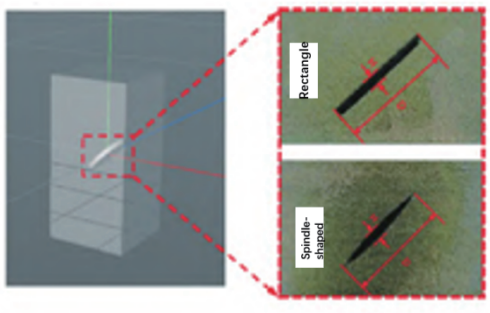


Figure 6 Fracture shapes [20]

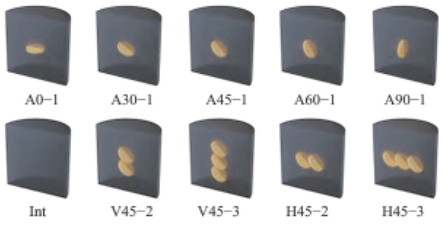


Figure 7 Different dip angles and numbers of fractures [21]

A recent development is the work of Hu et al. [6], who used emulsion-based proppants to fabricate internal open fractures in a magnesium phosphate cement binder-jetting system containing quartz sand. Their comparison showed higher peak strength for filling-type fractured specimens than for open-type counterparts under uniaxial compression. This cement-based powder system should be distinguished from conventional sand-resin printing. The filling state of a printed discontinuity therefore needs to be identified before its mechanical response is interpreted.

4.2 Mechanical Effects of Infilled Fractures

Open and infilled fractures follow different fabrication routes. An open fracture is defined in the digital model as a thin unbonded region; after printing, the loose powder is removed through the fracture outlet or an access channel. For a fully internal fracture, a removable support is required: Hu et al. [6] used emulsion-based proppants that were removed after curing to leave an open internal fracture. An infilled fracture is printed as a separate material region within the matrix. The filling geometry is defined in the model, and the filling mixture, binder content, and cementation degree are

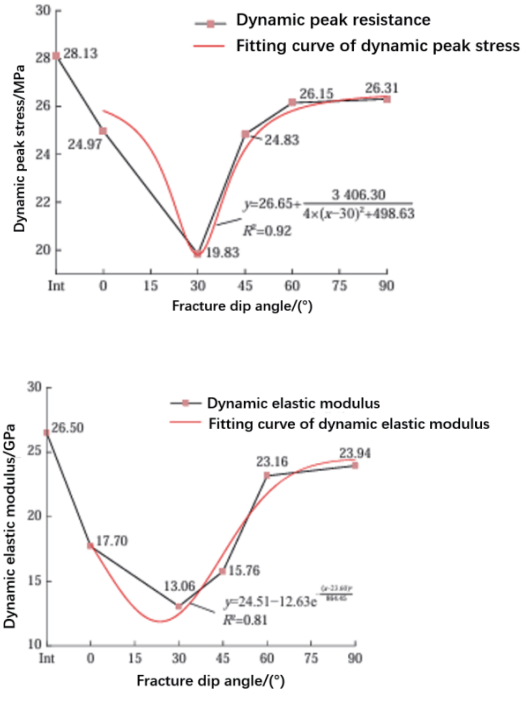


Figure 8 Dynamic peak stress and dynamic elastic modulus of specimens with different fracture dip angles [21]. Int = intact specimen.

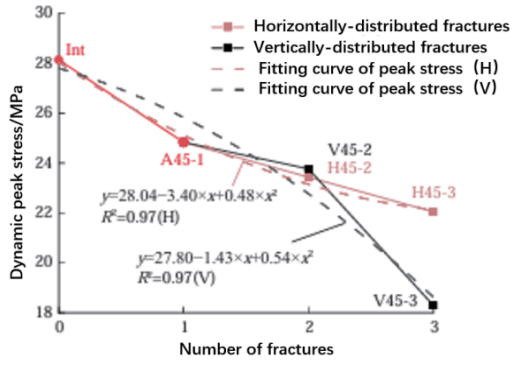


Figure 9 Dynamic peak stress of specimens with different numbers and distributions of fractures [21]. Int = intact specimen.

varied independently; the filling and matrix bond during printing, so the interface is part of the specimen. This route reproduces filling thickness, filling strength, and cementation degree, which control whether the fracture slips, transfers stress, or arrests cracks.

Natural fractures are often filled with materials such as clay, calcite, cemented particles, or crushed rock fragments. The mechanical response of an infilled fracture differs from that of an open fracture because the filling material can transfer stress, resist closure, and affect crack propagation. Sand powder 3D printing allows the filling condition of fractures to be controlled more accurately, including filling thickness, filling strength, and cementation degree [2].

Studies on infilled fractured specimens show that the cementation condition of the fracture filling strongly influences strength and failure mode. When the filling is weakly cemented, the fracture behaves as a dominant weak plane, and failure tends to occur by sliding or splitting along the filled fracture. As the cementation degree increases, the fracture becomes more capable of transferring stress, and specimen strength and stiffness increase accordingly. When the cementation degree reaches a relatively high level, the failure mode may change from fracture-controlled shear failure to more distributed tensile splitting failure [2].

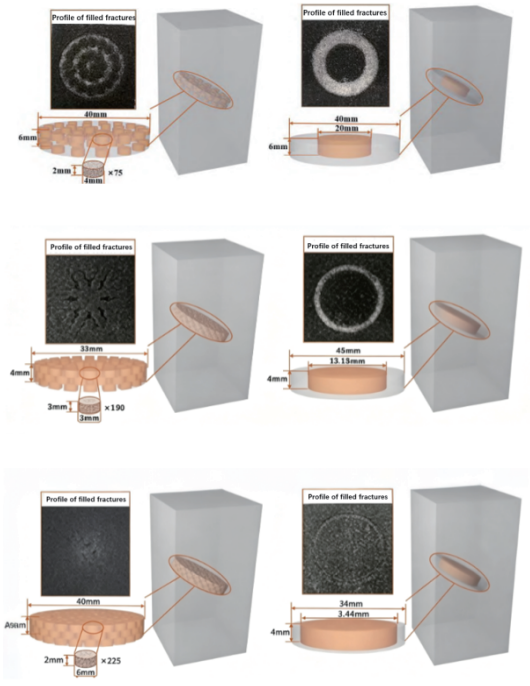


Figure 10 Cross-sections of specimens with different fracture-filling methods [2]

This indicates that filling materials do not simply weaken a rock mass. Their effect depends on the bonding quality between the filling and the surrounding matrix. Therefore, studies of infilled fractures should consider both geometric discontinuity and mechanical discontinuity [2].

Residual powder and binder migration change the mechanical state of a printed discontinuity. Hu et al. [6] measured higher peak strength in filled specimens than in open specimens and observed different crack paths, which shows that the filling state changes the mechanical response.

4.3 Implications for Fracture-Controlled Rock Failure

The main value of sand powder 3D printing in fractured rock mechanics lies in its ability to build repeatable specimens with controllable defects. This allows researchers to separate the effects of fracture geometry, fracture filling, and matrix properties. As a result, the progressive failure process can be analyzed more clearly than in tests using natural rocks [2, 20].

The same fabrication control allows fracture angle, length, spacing, and filling state to be varied independently, so crack initiation, propagation, and coalescence can be compared under otherwise identical conditions. This is the main experimental advantage of printed fractured specimens over natural rock samples.

5 Engineering Applications of Sand Powder 3D-Printed Rock Analogs

Sand powder 3D printing is useful for physical models in which roadway geometry, strata, and pre-existing fractures must be reproduced consistently. In a roadway study based on field-measured fracture parameters, Wang et al. [7] prepared intact and fractured surrounding-rock models using sand printing and examined them under biaxial loading with digital image correlation (DIC). Failure in the fractured model developed preferentially along the prefabricated fractures, while the intact model showed a different pattern of damage around the roadway. This supports the use of printed models to investigate how a specified fracture arrangement affects deformation and failure. The result should be interpreted within the material properties and loading conditions of that experiment.

Scale effects must be assessed before transferring specimen results to a roadway model or field setting. In a sand powder

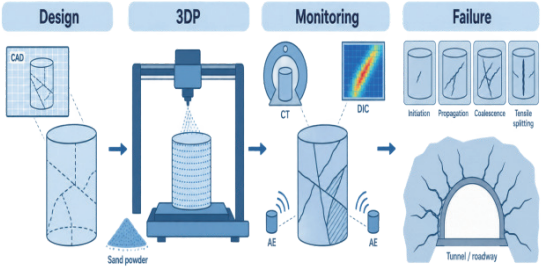


Figure 11 Sand powder 3D printing for fracture reconstruction and failure analysis

printing study of fractured specimens, Wang et al. [23] reported that, for specimens containing a 90° fracture, uniaxial compressive strength decreased from 7.39 MPa at a specimen width of 50 mm to 5.41 MPa at 100 mm. The fracture dimensions were scaled with specimen size, yet the measured strength changed by approximately 27%. This is evidence of a size effect within the tested specimen series, not a conversion factor for all printed roadway models. Future model designs should compare several sizes while keeping the intended geometric ratios and material preparation consistent, and should examine whether normalized strength, displacement, and failure patterns converge.

For a scaled roadway model, geometric resemblance should be accompanied by a stated similarity scheme. The scheme should identify the ratios for roadway dimensions, layer thicknesses, fracture length and spacing, unit weight, applied stress, strength, stiffness, and deformation. Where gravity-induced stress is a governing condition, the required stress ratio depends on the unit-weight and length ratios; externally applied boundary loads must then be selected consistently with the target stress state. Support studies additionally require attention to bolt or cable spacing, axial stiffness, interface bonding, and installation sequence. Tests on bolted sand powder specimens under combined static and dynamic loading demonstrate that this technology can examine reinforcement effects, but those specimen results alone do not validate a supported roadway at engineering scale [25].

The contribution of these models should be assessed through the documented relationship between the printed material, the modeled structure, and the engineering prototype. This review recommends reporting geometric scaling, material-property calibration, loading paths, boundary constraints, and the representation of support elements, together with the actual fracture geometry and filling state. These are proposed evaluation requirements, rather than conditions demonstrated to have been satisfied by every published model. Where scaling relationships or field comparisons remain incomplete, results should be interpreted as evidence of mechanisms under the tested conditions, with the limits of engineering extrapolation stated explicitly.

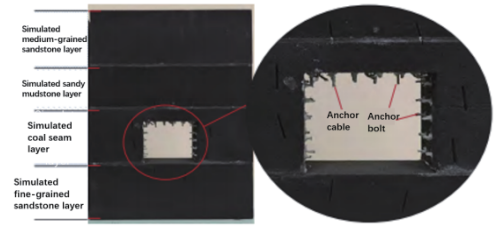


Figure 12 Physical model for simulating support of fractured surrounding rock [7]

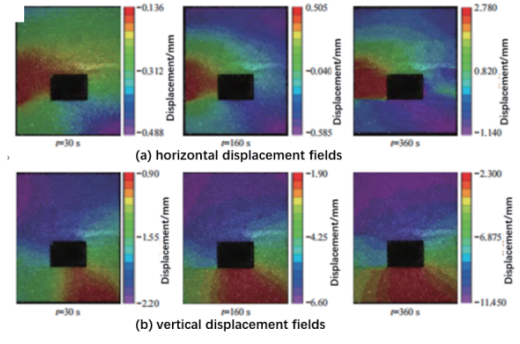


Figure 13 DIC displacement fields during deformation of a fractured roadway model [7]. (a) Horizontal displacement fields; (b) vertical displacement fields.

6 Summary

Future work should first establish a scale-specific validation procedure. Printed specimens and roadway models should be prepared at multiple sizes using the same material system and proportional fracture layouts. Tests should report how compressive strength, stiffness, crack initiation, normalized displacement, and failure mode vary with size. This would help determine the range over which results remain comparable and identify when the fixed particle size or printing layer thickness becomes too large relative to a scaled geological feature. The size-dependent strength reported by Wang et al. [23] illustrates why this check is necessary.

Material development should be guided by the target engineering process. Before printing a complete model, candidate mixtures should be tested for compressive and tensile strength, elastic modulus, stress–strain response, and post-peak behavior under relevant loading conditions. Fracture orientation, filling state, and interlayer properties should be measured on the finished specimens. For supported models, the mechanical response of the bolt–rock interface should also be calibrated. A material that matches a target compressive strength under uniaxial loading may respond differently under confinement; triaxial tests on fractured sand powder analogs provide a basis for extending this validation [22].

Loading systems should progress from simple compression to controlled simulation of the intended stress path. Priorities include independently applied boundary stresses, excavation-induced unloading, and combined static and dynamic loading where these occur in the prototype. Each experiment should document boundary restraint and loading sequence so that their effects can be separated from the effects of fracture geometry or support. Parallel numerical models can then be calibrated with the measured material and interface properties and used to test which conclusions are sensitive to boundary assumptions.

Finally, printing and measurement improvements should be evaluated together. Finer control of powder gradation, layer thickness, binder deposition, curing, and internal powder removal may improve the reproduction of small fractures and reduce variation between specimens. CT should verify internal geometry and filling before testing; synchronized DIC and acoustic emission should relate surface deformation and damage activity to load history; and post-test CT should locate internal crack growth. Reporting geometric errors, property variation across repeated prints, and differences between measured and predicted failure locations would make the practical accuracy of an engineering model assessable rather than assumed.

Acknowledgements

The authors would like to thank the editor and the anonymous reviewers for their constructive comments and suggestions, which helped improve the quality of this manuscript. This research did not receive any specific grant from funding agencies in the public, commercial, or not-for-profit sectors.

Declaration of competing interest

The authors have no competing interests to declare that are relevant to the content of this article.

Author contributions

Aoyu Li: Data curation, Formal analysis, Visualization, Writing – original draft (including translation). **Lishuai Jiang**: Conceptualization, Investigation, Supervision, Writing – review & editing. **Zhe Zhang**: Resources, Supervision. **Hani Mitri**: Investigation, Resources, Supervision.

Data availability

This is a review article. No new data were generated or analysed in this study. All data and materials discussed in this review are available in the publications cited in the article, and further information can be obtained from the corresponding author upon reasonable request.

Use of AI statement

During the preparation of this work, the authors used DeepSeek and ChatGPT to translate the manuscript from Chinese into English and to improve the language and readability of the text, including the descriptive text accompanying Fig. 1. After using these tools, the authors reviewed and edited all AI-assisted output, checked the translated content against the original manuscript and the cited literature, and take full responsibility for the content of the published article. The AI tools were used solely for translation and language polishing; they did not generate scientific content, data, analyses, or conclusions, and they are not listed as authors or co-authors.

References

[1] Zhang, Z.; Jiang, L. S.; Li, C. N.; Zhao, Y.; Sainoki, A.; Gong, X. L. Characteristics and mechanism of time on sand powder 3D printing rock analogue: a new method for fractured rock mechanics. *Geomech. Geophys. Geo-Energy Geo-Resour* **2023**, *9*, 166.

[2] Wang, X. Z.; Jiang, L. S.; Li, Y. Y.; Zhang, L.; Sainoki, A.; Mitri, S. H.; Yang, Y. M.; Peng, X. H. Experimental study on the mechanical behavior and failure characteristics of rock analogs with filled internal fractures: a new method by sand powder 3D printing. *Constr. Build. Mater* **2024**, *427*, 136261.

[3] Braun, P.; Tzortzopoulos, G.; Stefanou, I. Design of sand-based, 3-D-printed analog faults with controlled frictional properties. *J. Geophys. Res.: Solid Earth* **2021**, *126*, e2020JB020520.

[4] Jiang, L. S.; Wang, X. Z.; Xu, Q.; Xu, J. R.; Liu, G. S. Influence and mechanism of printing materials on the mechanical properties of sand powder 3D printed weak rock-like materials. *Coal Sci. Technol* **2023**, *51*, 84–94 (in Chinese), doi: 10.12438/cst.2022-2060.

[5] Yu, C.; Tian, W. Application and prospective of sand-type 3D printing material in rock mechanics: a review. *Rapid Prototyp. J* **2024**, *30*, 1057–1069.

[6] Hu, T. Y.; Dou, C. Y.; Cheng, Z.; Ma, G. W.; Li, Z. J. Fabrication of internal 3D open-type fractures in binder jetting 3D printed rock matrix using emulsion-based proppants. *Theor. Appl. Fract. Mech* **2025**, *140*, 105202.

[7] Wang, Z. K.; Jiang, L. S.; Liu, Y. L.; He, X.; Zhao, W. S.; Huang, Y. F. Deformation and failure behavior of fractured rock roadway: physical simulation with 3D printing. *J. Min. Strata Control Eng* **2025**, *7*, 033512 (in Chinese).

[8] Wu, X. Y.; Tao, M.; Yang, Z.; Xiao, Z. H.; Zhao, R.; Wang, S. F. Stress migration and failure mechanisms of rocks with holes under gradient stress conditions. *Int. J. Rock Mech. Min. Sci* **2025**, *195*, 106306.

[9] Wu, X. Y.; Tao, M.; Sainoki, A.; Jiang, L. S.; Zhao, R. Mechanical response and failure mechanism of rock with holes under multiple stress gradients. *Rock Mech. Rock Eng*. **2026**. in press, DOI: 10.1007/s00603-026-05283-8.

[10] Gao, Y. T.; Wu, T. H.; Zhou, Y. Application and prospective of 3D printing in rock mechanics: a review. *Int. J. Miner. Metall. Mater* **2021**, *28*, 1–17.

[11] Jiang, L. S.; Gao, M. T.; Wang, Z. K.; Zhao, Y.; Feng, H.; Zhang, Z.; Cai, D. S.; Li, G. C. Research progress on physical reconstruction of coal-rock mass and roadway model test based on sand-powder 3D printing. *J. Min. Strata Control Eng* **2026**, *8*, 023011 (in Chinese).

[12] Jiang, L. S.; Zhao, Y.; He, X.; Zhao, Y.; Li, P. M.; Wang, Z. K.; Guo, D. R. Experimental research on the glass fiber-reinforced effect and mechanisms of sand powder 3D-printed rock-like materials. *J. Mater. Res. Technol* **2024**, *33*, 1971–1983.

[13] Zhang, Z.; Jiang, L. S.; Sainoki, A.; Peng, X. H.; Li, C. N.; Niu, Q. J.; Wang, X. Z.; Gang, M. Strengthening effect of particle gradation on the mechanical properties of sand powder 3D printed rock analog. *J. Mater. Res. Technol* **2025**, *35*, 1377–1390.

[14] Wang, Y.; Li, S. J.; Song, R.; Liu, J. J.; Ye, M.; Peng, S. Q.; Deng, Y. J. Effects of grain size and layer thickness on the physical and mechanical properties of 3D-printed rock analogs. *Energies* **2022**, *15*, 7641.

[15] Xu, Q.; Jiang, L. S.; Ma, C. Q.; Niu, Q. J.; Wang, X. Z. Effect of layer thickness on the physical and mechanical properties of sand powder 3D printing specimens. *Front. Earth Sci* **2021**, *9*, 763202.

[16] Jiang, L. S.; Peng, X. H.; Golsanami, N.; Zhao, Y.; Zhang, Z.; Xu, Q. Research progress on material development and forming technology of high mechanical similarity 3D printing coal-like rock. *J. China Coal Soc* **2026**, *51*, 1135–1149 (in Chinese).

[17] Perras, M. A.; Vogler, D. Compressive and tensile behavior of 3D-printed and natural sandstones. *Transp. Porous Med* **2019**, *129*, 559–581.

[18] Song, R.; Wang, Y.; Ishutov, S.; Zambrano-Narvaez, G.; Hodder, K. J.; Chalaturnyk, R. J.; Sun, S. Y.; Liu, J. J.; Gamage, R. P. A comprehensive experimental study on mechanical behavior, microstructure and transport properties of 3D-printed rock analogs. *Rock Mech. Rock Eng* **2020**, *53*, 5745–5765.

[19] Zhuang, D. Y.; Ning, Z. X.; Chen, Y. M.; Li, J. L.; Li, Q. D.; Xu, W. J. Investigation on mechanical properties regulation of rock-like specimens based on 3D printing and similarity quantification. *Int. J. Min. Sci. Technol* **2024**, *34*, 573–585.

[20] Jiang, L. S.; Wu, Q.; Gao, M. T.; Yang, Y. M.; Wu, C. L.; Li, H. Z. Experimental study on influence of internal crack geometrical features on mechanical properties of rock-like specimens. *J. Shandong Univ. Sci. Technol. (Nat. Sci.)* **2026**, *45*, 12–25 (in Chinese).

[21] Jiang, L. S.; Yang, Y. M.; Zhao, Y.; Li, H. Z.; Wu, Q.; Peng, X. H. Mechanical response and energy dissipation law of rock-like mass with internal fractures under dynamic load. *Coal Sci. Technol* **2025**, *53*, 137–150 (in Chinese).

[22] Li, P. M.; Jiang, L. S.; Wen, Z. J.; Wu, C. L.; Yang, Y. M.; Peng, X. H.; Wu, Q. S.; Wu, Q. L. Effect of fractures on mechanical behavior of sand powder 3D printing rock analogue under triaxial compression. *J. Cent. South Univ* **2024**, *31*, 2703–2716.

[23] Wang, W. H.; Zhao, Y.; Jiang, L. S.; Zuo, J. C.; Liu, G. S.; Mitri, H. S. Preliminary study on size effect of fractured rock mass with sand powder 3D printing. *Processes* **2022**, *10*, 1974.

[24] Cheng, Z.; Zhang, Y. Y.; Hu, T. Y.; Li, Z. J.; Ma, G. W. Fractured rock analogs by binder jetting 3D printing using cement: improvements in geometric similarity and mechanical performance. *Addit. Manuf* **2025**, *111*, 104976.

[25] Wu, X. Y.; Jiang, L. S.; Tao, M.; Mitri Hani, S.; Xiang, G. L. Dynamic behaviors and bolt-strengthening effect of sand-powder 3D printing rock analog under static and dynamic coupled loading. *Constr. Build. Mater* **2024**, *411*, 134723.

This is an open access article under the terms of the Creative Commons Attribution 4.0 International License (CC BY 4.0, https://creativecommons.org/licenses/by/4.0/).

© The Author(s) 2026. Published by Tsinghua University Press.